The Assimilation of Observations from the Advanced Microwave Sounding Unit over Sea Ice in the French Global Numerical Weather Prediction System

FATIMA KARBOU

CNRM-GAME, Météo-France/CNRS, Saint Martin d'Hères, France

FLORENCE RABIER

CNRM-GAME, Météo-France/CNRS, Toulouse, France

CATHERINE PRIGENT

Observatoire de Paris, Paris, France

(Manuscript received 17 January 2013, in final form 9 August 2013)

ABSTRACT

The aim of this study is to test the feasibility of assimilating microwave observations from the Advanced Microwave Sounding Units (AMSU-A and AMSU-B) through the implementation of an appropriate parameterization of sea ice emissivity. AMSU observations are relevant to the description of air temperature and humidity, and their assimilation into numerical weather prediction (NWP) helps better constrain models in regions where very few observations are assimilated. A sea ice emissivity model suitable for AMSU-A and AMSU-B data is described in this paper and its impact is studied through two assimilation experiments run during the period of the Arctic winter. The first experiment is representative of the operational version of the Météo-France NWP model whereas the second simulation uses the sea ice emissivity parameterization and assimilates a selection of AMSU channels above polar regions. The assimilation of AMSU observations over sea ice is shown to have a significant effect on atmospheric analyses (in particular those of temperature and humidity). The effect on temperature induces a warming in the lower troposphere, especially around 850 hPa. This leads to an increase in the Arctic inversion strength over the ice cap by almost 2 K. An improvement in medium-range forecasts is also noticed when the NWP model assimilates AMSU observations over sea ice.

1. Introduction

Concordiasi is an international project that is part of the International Polar Year (IPY) The Observing System Research and Predictability Experiment (THORPEX) program (Rabier et al. 2010, 2013). During this project, different types of observations are used over polar regions and innovative methods are developed for surface and atmospheric modeling. In particular, several studies were conducted, as part of Concordiasi, to improve analyses–forecasts over polar regions by the assimilation of new data, to improve the use of remote sensing observations, to enhance the observation network, and to study the Antarctic ozone layer and its potential interactions with lower latitudes. Although the polar regions are well covered by polar-orbiting satellites, very few remote sensing observations are really used in data assimilation systems. This is even more true over sea ice. The representation of the emissivity of sea ice is one of the factors limiting the assimilation of observations on this type of surface (English 2008). Studies focusing on the modeling of snow and sea ice emissivity were conducted within the framework of Concordiasi, to improve the use of microwave remote sensing observations in numerical weather prediction (NWP). Guedj et al. (2010) studied the impact of the reflection assumptions on the emissivity: specular, Lambertian, or using different specularity parameters following previous studies about the role of surface approximations on the emissivities estimated from remote sensing observations (Matzler 2005; Matzler and Rosenkranz 2007; Karbou

Corresponding author address: Fatima Karbou, CNRM-GAME, Météo-France/CNRS, 1441 Rue de la Piscine, Saint Martin d'Hères 38400, France.
E-mail: fatima.karbou@meteo.fr

DOI: 10.1175/MWR-D-13-00025.1

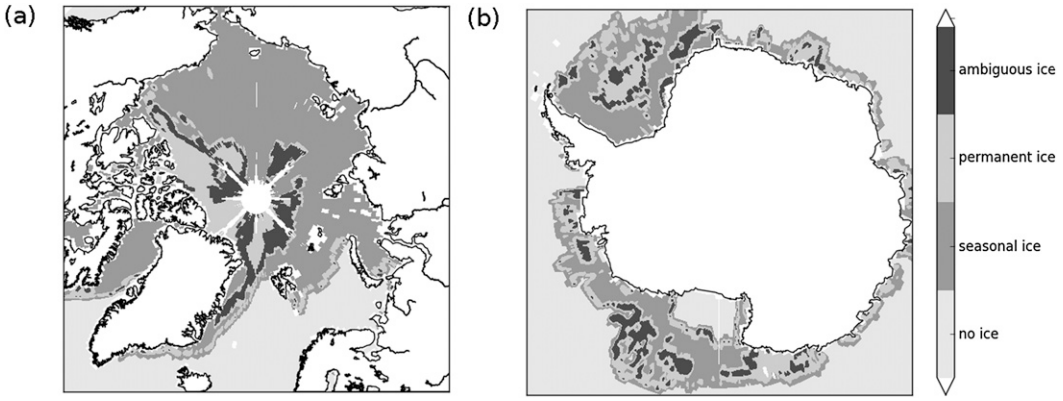

FIG. 1. Daily mean maps of sea ice types as provided by OSISAF for the (a) Northern and the (b) Southern Hemispheres, dated 5 Jan 2009.

and Prigent 2005). In addition, developments have been tested to increase the number of satellite observations assimilated over Antarctica (infrared and microwave) and over the surrounding sea ice (Bouchard et al. 2010). The method previously developed by Karbou et al. (2006) to estimate the microwave emissivity of land surfaces within the French NWP model has been applied to cold areas (land and sea ice), which allowed the assimilation of Advanced Microwave Sounding Unit (AMSU) observations over Antarctica and its surrounding sea ice. Although satisfactory results have been obtained from these developments, there is still a strong need for an improved modeling of sea ice emissivity, especially at higher frequencies (starting from 89 GHz). This article focuses on developments specific to sea ice emissivity, which acts directly on the increase of the number of assimilated observations over polar regions. Thus, the emissivity of sea ice has been calculated for several frequencies: 23, 31, 50, 89, and 150 GHz. The variability of the emissivity in space and time was studied. The analysis of its variability in frequency was undertaken, whereby a new parameterization of sea ice emissivity dedicated to the AMSU-A and -B measurement with a view toward assimilating them into an NWP model was tested. Data and methods are introduced in section 2. Section 3 is dedicated to the estimation and the study of the emissivity of sea ice. In section 4, we discuss the impact of a sea ice emissivity scheme within the framework of NWP. Section 5 summarizes the results found in this study.

2. Parameterizing the sea ice emissivity

a. Remote sensing microwave observations

The AMSU-A and -B instruments are part of the most widely used remote sensing instruments in data assimilation for numerical weather prediction thanks to their measurements providing information on the vertical structure of the air temperature and humidity. The AMSU-A sensor measures in 15 frequencies from 23.8 to 89 GHz. It has 11 sounding channels near the oxygen absorption band (50–60 GHz) for temperature sounding from the surface to almost 45-km height. AMSU-A has four other channels more sensitive to the surface (23.8, 31.4, 50.8, and 89 GHz). AMSU-B is designed for tropospheric humidity retrievals using three channels centered on the strong 183.31-GHz water vapor line. The instrument has two other channels, usually called window channels, at 89 and 150 GHz, which are mainly sensitive to the surface and to low atmospheric layers. The reader is invited to read Goodrum et al. (2012) for further details about these instruments. We also used the European Organisation for the Exploitation of Meteorological Satellites (EUMETSAT) Ocean and Sea Ice Satellite Application Facility (OSISAF) sea ice classification data derived from the Special Sensor Microwave Imager (SSM/I). Andersen et al. (2012) give a description of the OSISAF products. Figure 1 shows ice-type classification maps for 5 January 2009 in the Northern and the Southern Hemispheres.

b. The emissivity retrieval

To estimate the sea ice emissivity, a method similar to that of Karbou et al. (2006) for NWP application is used

TABLE 1. List of window channels for which the sea ice emissivity was computed.

Instrument	Channel No.	Frequency (GHz)
AMSU-A	1	23.8
	2	31.4
	3	50.3
	15	89
AMSU-B	1	89
	2	150

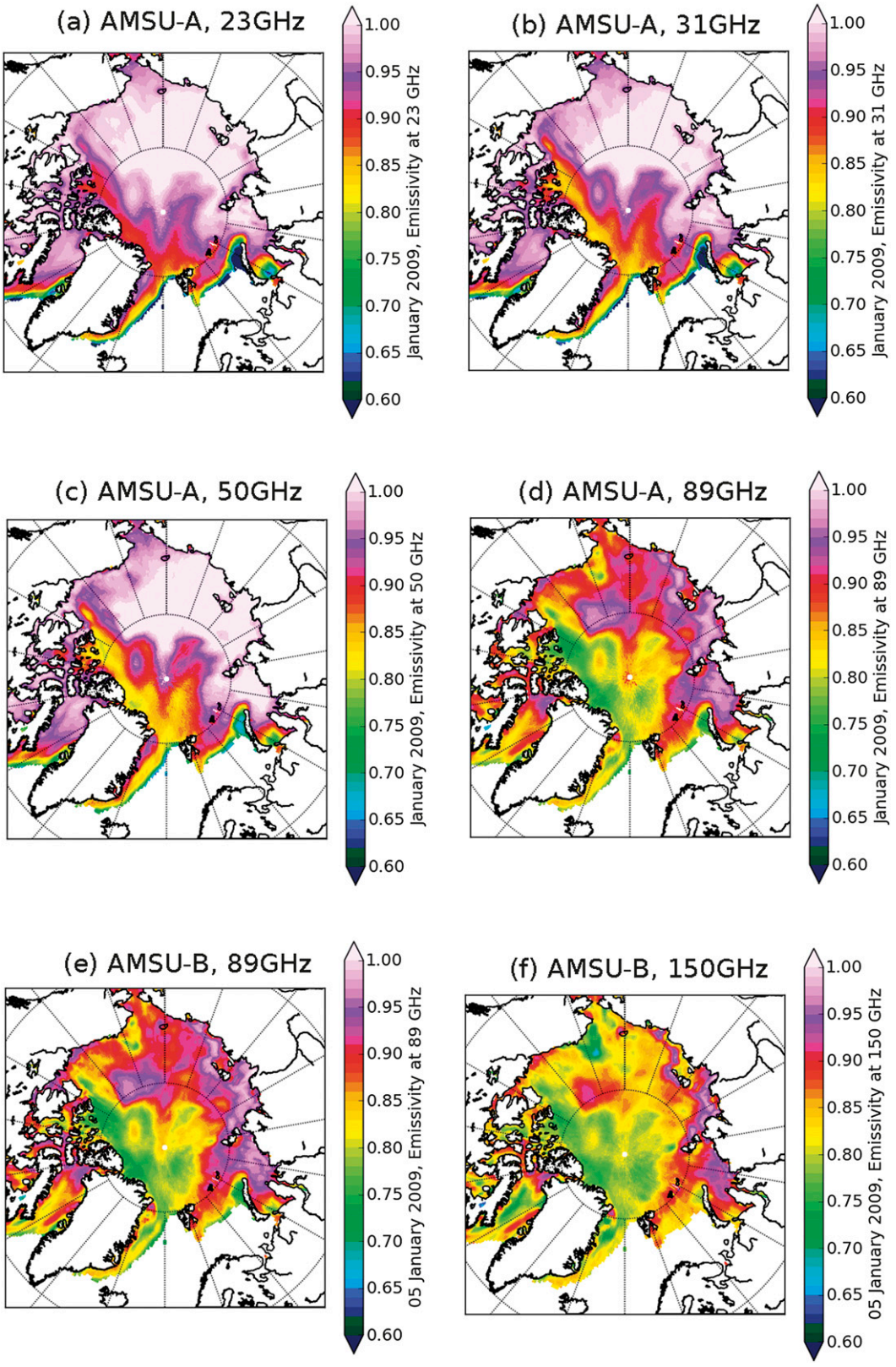

FIG. 2. Monthly mean emissivity maps estimated above the sea ice in the Northern Hemisphere using AMSU-A and AMSU-B window channel measurements during January 2009 at (a) 23, (b) 31, (c) 50, (d) 89, (e) 89, and (f) 150 GHz.

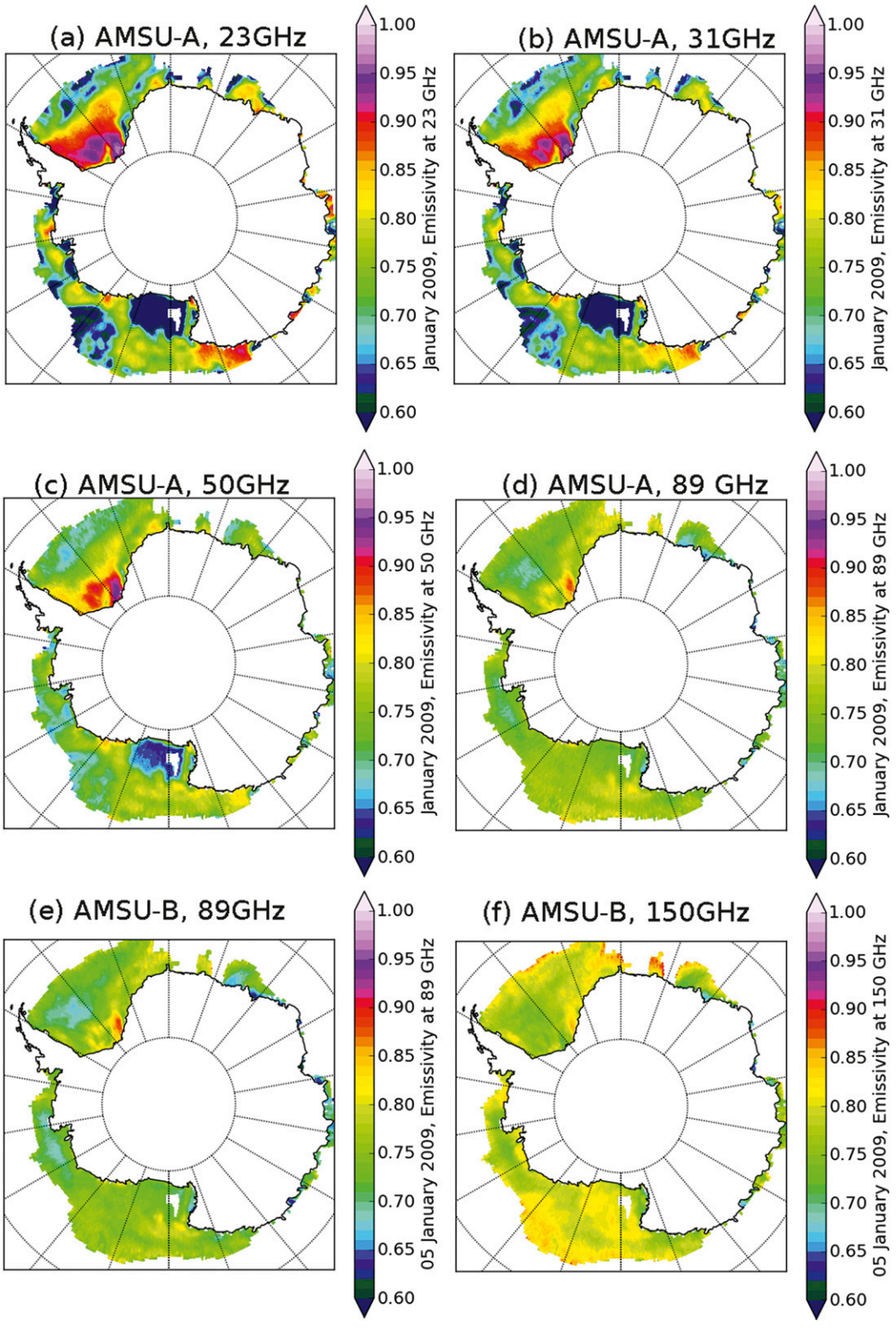

FIG. 3. As in Fig. 2, but for sea ice surfaces in the Southern Hemisphere.

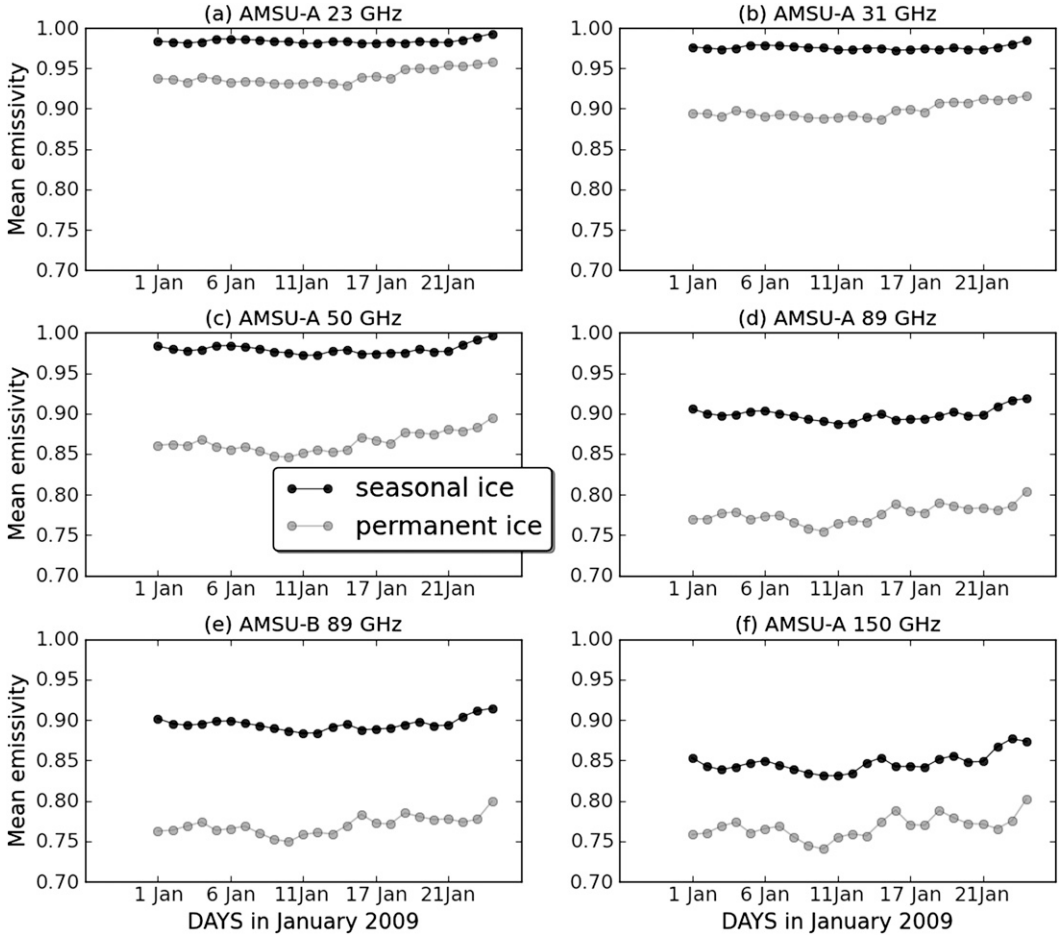

FIG. 4. Daily time series of emissivity estimates derived using measurements from AMSU-A and AMSU-B in the Northern Hemisphere for two sea ice types: seasonal ice (black) and permanent ice (gray). Results are given for the period ranging from 1 to 24 Jan 2009 and for (a) 23, (b) 31, (c) 50, (d) 89, (e) 89, and (f) 150 GHz.

for frequencies from 23 to 150 GHz. The method is based on the following assumptions: the atmosphere can be considered nonscattering and plane parallel, the surface is specular, and the medium emits at the temperature of the surface skin. Using these assumptions, the radiometric signal received by the satellite can be decomposed into three parts: 1) emission by the top of the atmosphere, 2) a second part emitted/attenuated by successive layers of the atmosphere and reflected by the surface, and 3) surface emission, which depends on the surface emissivity and the surface temperature partly absorbed by the atmosphere. Using these assumptions and for a given AMSU zenith angle and frequency, the brightness temperatures (noted T_b, hereafter) observed by the sensor can be expressed as

$$T_b(\nu,\theta) = T_s\varepsilon(\nu,\theta)\Gamma + [1-\varepsilon(\nu,\theta)]\Gamma T_a^{\downarrow}(\nu,\theta) + T_a^{\uparrow}(\nu,\theta)$$
$$\Gamma = \exp\left[\frac{-\tau(0,H)}{\cos(\theta)}\right], \tag{1}$$

where $T_b(\nu,\theta)$ and $\varepsilon(\nu,\theta)$ represent the T_b measured by the sensor and the surface emissivity at frequency ν and at observation zenith angle θ, respectively; T_s, $T_a^{\downarrow}(\nu,\theta)$, and $T_a^{\uparrow}(\nu,\theta)$ are the skin temperature and the atmospheric downwelling and upwelling temperatures, respectively; Γ is the net atmospheric transmissivity and can be expressed as a function of the atmospheric opacity $\tau(0, H)$ and the observation zenith angle θ; and H is the top-of-the-atmosphere height.

The microwave land emissivity can then be retrieved as follows:

$$\varepsilon(\nu,\theta) = \frac{T_b(\nu,\theta) - T_a^{\uparrow}(\nu,\theta) - T_a^{\downarrow}(\nu,\theta)\Gamma}{[T_s - T_a^{\downarrow}(\nu,\theta)]\Gamma}. \tag{2}$$

The emissivity can be estimated from the observed brightness temperatures from a priori information about the atmospheric contribution to the signal and the surface temperature. The commonly used approach is to

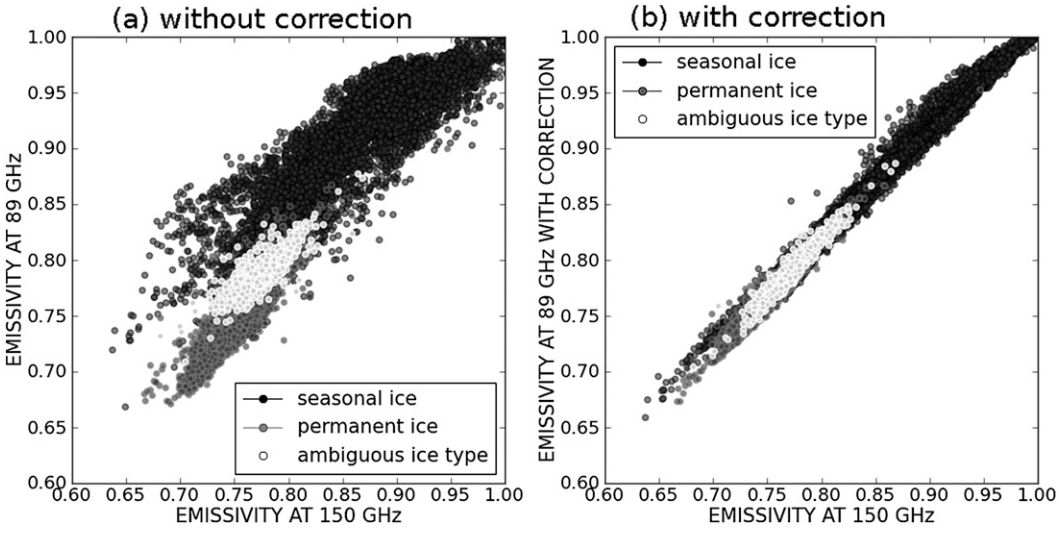

FIG. 5. Scatterplots of daily sea ice emissivities in the Northern Hemisphere as a function of the OSISAF sea ice types for 1 Jan 2009. Results are for (a) emissivity at 89 vs 150 GHz and (b) 89-GHz emissivity extrapolated at 150 GHz vs emissivity at 150 GHz.

estimate the atmospheric contribution to the signal using a forward radiative transfer model whose input parameters include air temperature and humidity profiles from short-range forecasts and surface temperature estimates from these forecasts or from an independent database (see, e.g., Felde and Pickle 1995; Choudhury 1993; Jones et Vonder Haar 1997; Prigent et al. 1997; Prigent et al. 2000, 2005; Karbou et al. 2005; Mathew et al. 2008, 2009, among others).

This study uses the method described in Karbou et al. (2006): short-range forecasts of surface temperature and of air temperature and humidity from the Action de Recherche Petite Echelle Grande Echelle (ARPEGE) model used as input for the Radiative Transfer for Television and Infrared Observation Satellite (TIROS) Operational Vertical Sounder (RTTOV) model (Eyre 1991; Saunders et al. 1999; Matricardi et al. 2004) and emissivity calculated for all AMSU-A and AMSU-B window channels (listed in Table 1). Figure 2 shows monthly mean emissivity maps in the Northern Hemisphere for January 2009 obtained from selected window channels (listed in Table 1): (a) AMSU-A 23.8 GHz, (b) AMSU-A 31.4 GHz, (c) AMSU-A 50.3 GHz, (d) AMSU-A 89 GHz, (e) AMSU-B 89 GHz, and (f) AMSU-B 150 GHz. Figure 3 shows the same monthly mean emissivity maps but for the Southern Hemisphere. During the month of January 2009 almost 80% of the Arctic sea ice was seasonal and, as expected, the emissivity of sea ice in both hemispheres shows a strong variability in space and frequency. Low emissivity values are observed in the boundary areas between sea ice and open water. These areas are also associated with higher values of emissivity standard deviation during the month of January. To be noted are the low values of emissivity (0.5) at frequencies below 50 GHz, which correspond to the open sea north of the Ross Sea in Antarctica (ice-free area in Fig. 1b). Regardless of the frequency, emissivity values are larger for seasonal ice than for permanent sea ice. More generally, the variability of the emissivity appears to be closely related to the type of sea ice. Figure 4 shows daily time series of emissivity derived from AMSU-A and AMSU-B window channels for seasonal ice (black) and for permanent sea ice (gray) calculated using all available data over the Northern Hemisphere. According to Fig. 4, and whatever the microwave frequency, the emissivity of the seasonal ice is higher than that of the permanent ice. The gap in emissivities between the two ice types is less at frequencies near 23 and 31 GHz compared to frequencies over 50 GHz (except 150 GHz). The emissivity difference is about 5% at lower frequencies while it reaches 10% at 50 and 89 GHz. This is consistent with the results of other recent studies (see, e.g., Kongoli et al. 2010; Mathew et al. 2009) examining the variability of the emissivity according to the frequency of the observations. Results in this section indicate that 1) the calculated emissivities of sea ice are of a good quality and reflect expected complex variations over sea ice and 2) the variability of the emissivity depends on many factors, including the age of the ice and this effect should be accounted for at high frequencies (89 and 150 GHz).

TABLE 2. Overview of the assimilation experiments.

Expt	Surface emissivity	Used AMSU over sea ice
CTL	Empirical formulation	AMSU-A, channels 7–14; AMSU-B channels, none
EXP	AMSU-A, emissivity derived at 50 GHz (AMSU-A channel 3); AMSU-B, emissivity derived at 89 GHz (AMSU-B channel 1) with a frequency dependence correction	AMSU-A, channels 5–14; AMSU-B, channels 3–5

c. *Sea ice emissivity for NWP*

A closer examination of the possible use of the emissivity to facilitate the assimilation of atmospheric sounding observations over sea ice will follow. Emissivity at 50 GHz (the closest window channel in frequency) seems the best suited for AMSU-A observations made at 52–55 GHz, which are sensitive to the temperature of the air. By contrast, for humidity-sensitive observations near 183 GHz, the use of emissivities at 89 GHz may introduce biases into the radiative transfer simulations because of the high and complex variability between 89 and 150 GHz of the emissivity (see previous section). It is also possible to use the emissivity at 150 GHz as a priori information for humidity sounding channels; however, this presents several disadvantages. First, the 150-GHz measurements are more sensitive to the atmosphere than are the measurements at 89 GHz; therefore, there is an increased risk of getting noisy emissivity estimates. Second, polar regions are often covered by clouds, which may also contribute to making the emissivity estimates noisier at 150 GHz. Third, as a quality control (QC) test is used in data assimilation to screen data contaminated by clouds, if the emissivity is calculated from the 150-GHz channel, this test can no longer be used. The QC test is based on the use of a threshold on differences between simulations and observations at 150 GHz according to whether or not the observations are accepted or rejected. If the emissivity is calculated at 150 GHz, the simulations will, by construction, be strictly identical to the observations. And, finally, the use of the 150-GHz channel to estimate the emissivity will prevent any assimilation trial of 150-GHz data over sea ice. Instead of retrieving emissivity at 150 GHz, a corrected 89-GHz emissivity better fitting the emissivity at 150 GHz is used. Figure 5a shows scatterplots of daily sea ice emissivities (emissivity at 89 GHz versus emissivity at 150 GHz) in the Northern Hemisphere as a function of sea ice types for 1 January 2009. It also shows a large discrepancy between the two emissivities and this disparity appears to be directly dependent on the ice type. There is a good amount of agreement between the emissivities at 89 and 150 GHz for permanent ice but strong differences appear for seasonal ice. Therefore, it is necessary to characterize these differences to extrapolate the 150-GHz emissivity from 89 GHz. As no information on this parameter is available in our assimilation system, the use of a proxy that could give

TABLE 3. AMSU-A and -B characteristics and conditions for use.

Instrument	Channel	Frequency (GHz)	Sensitivity	Conditions for use	Obs errors
AMSU-A	1	23.8	Surface	Not used	—
	2	31.4	Surface	Not used	—
	3	50.3	Surface	Not used	—
	4	52.8	Temperature	Not used	—
	5	53.596 ± 0.115	Temperature	Used	0.45
	6	54.4	Temperature	Used	0.35
	7	54.9	Temperature	Used	0.35
	8	55.5	Temperature	Used	0.35
	9	$\nu = 57.290$	Temperature	Used	0.35
	10	$\nu \pm 0.217$	Temperature	Used	0.35
	11	$\nu \pm 0.322 \pm 0.048$	Temperature	Used	0.50
	12	$\nu \pm 0.322 \pm 0.022$	Temperature	Used	0.80
	13	$\nu \pm 0.322 \pm 0.010$	Temperature	Used	1.2
	14	$\nu \pm 0.322 \pm 0.0045$	Temperature	Not used	—
	15	89	Surface	Not used	—
AMSU-B	1	89	Surface	Not used	—
	2	150	Surface	Not used	—
	3	183 ± 1	Humidity	Used	3.00
	4	183 ± 3	Humidity	Used	2.50
	5	183 ± 7	Humidity	Used	2.50

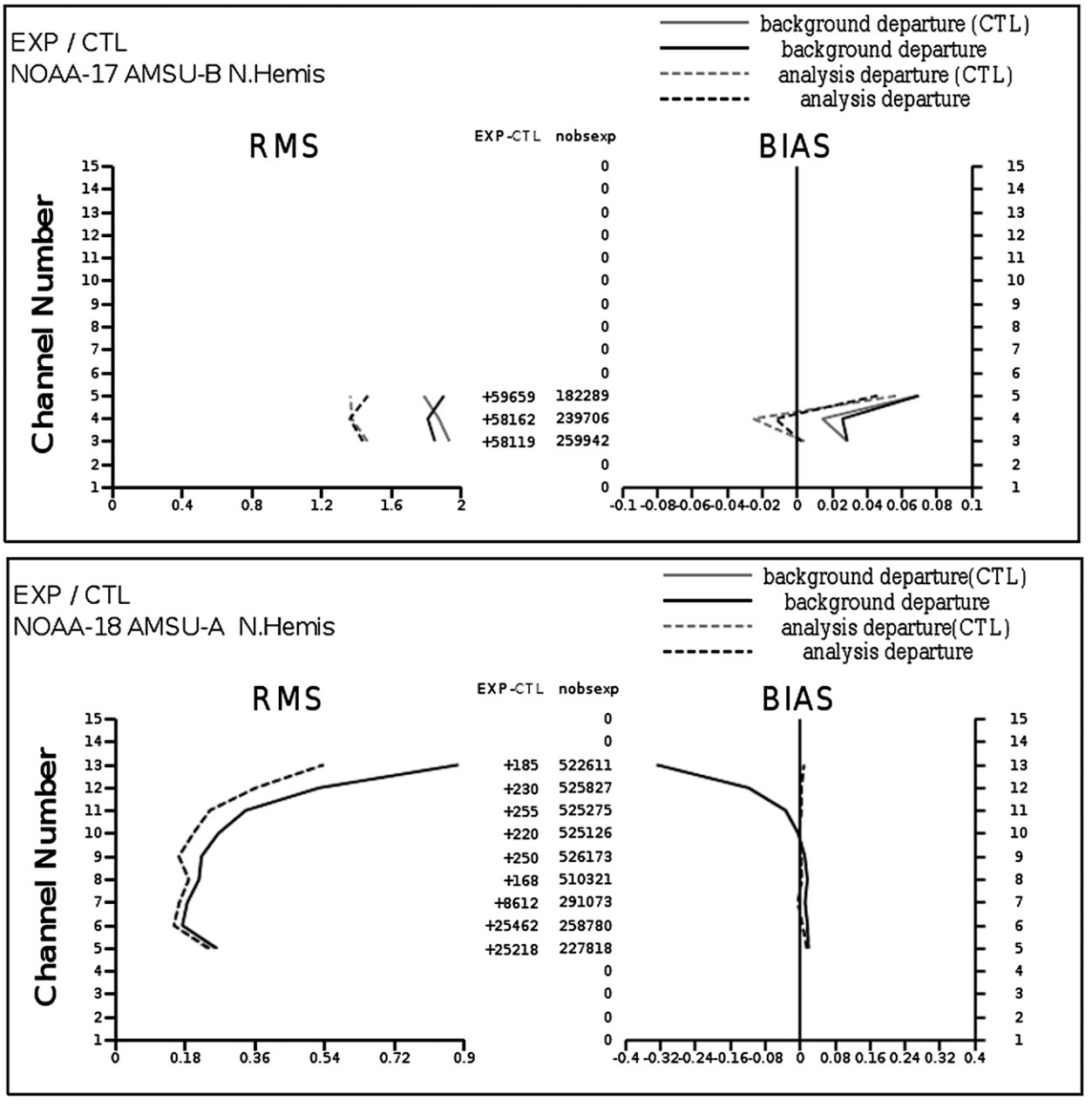

FIG. 6. (left) RMS error (K) and (right) bias (K) for the FGs (solid) and for the analysis departures (dashed) for assimilated (top) *NOAA-17* AMSU-B observations and (bottom) *NOAA-18* AMSU-A observations over the Northern Hemisphere for EXP (black) and CTL (gray). The period is January 2009.

indirect information was assessed to test the following extrapolation [obtained by neglecting the atmospheric contributions in Eq. (1) and assuming the transmission to be equal to 1]:

$$\varepsilon(150,\theta)_{\text{extrapolated}} = \varepsilon(89,\theta) - \frac{T_b(150,\theta) - T_b(89,\theta)}{T_s}, \tag{3}$$

where $\varepsilon(89, \theta)$ is the retrieved emissivity at 89 GHz; $T_b(89, \theta)$ and $T_b(150, \theta)$ are the observed T_bs at 89 and 150 GHz, respectively; and T_s is the surface temperature from the ARPEGE 6-h short-range forecasts. Figure 5b shows scatterplots of the obtained $\varepsilon(150, \theta)_{\text{extrapolated}}$ as a function of $\varepsilon(150, \theta)$. One can notice the very good agreement between both datasets, which suggests that the emissivity extrapolated from 89 to 150 GHz is better

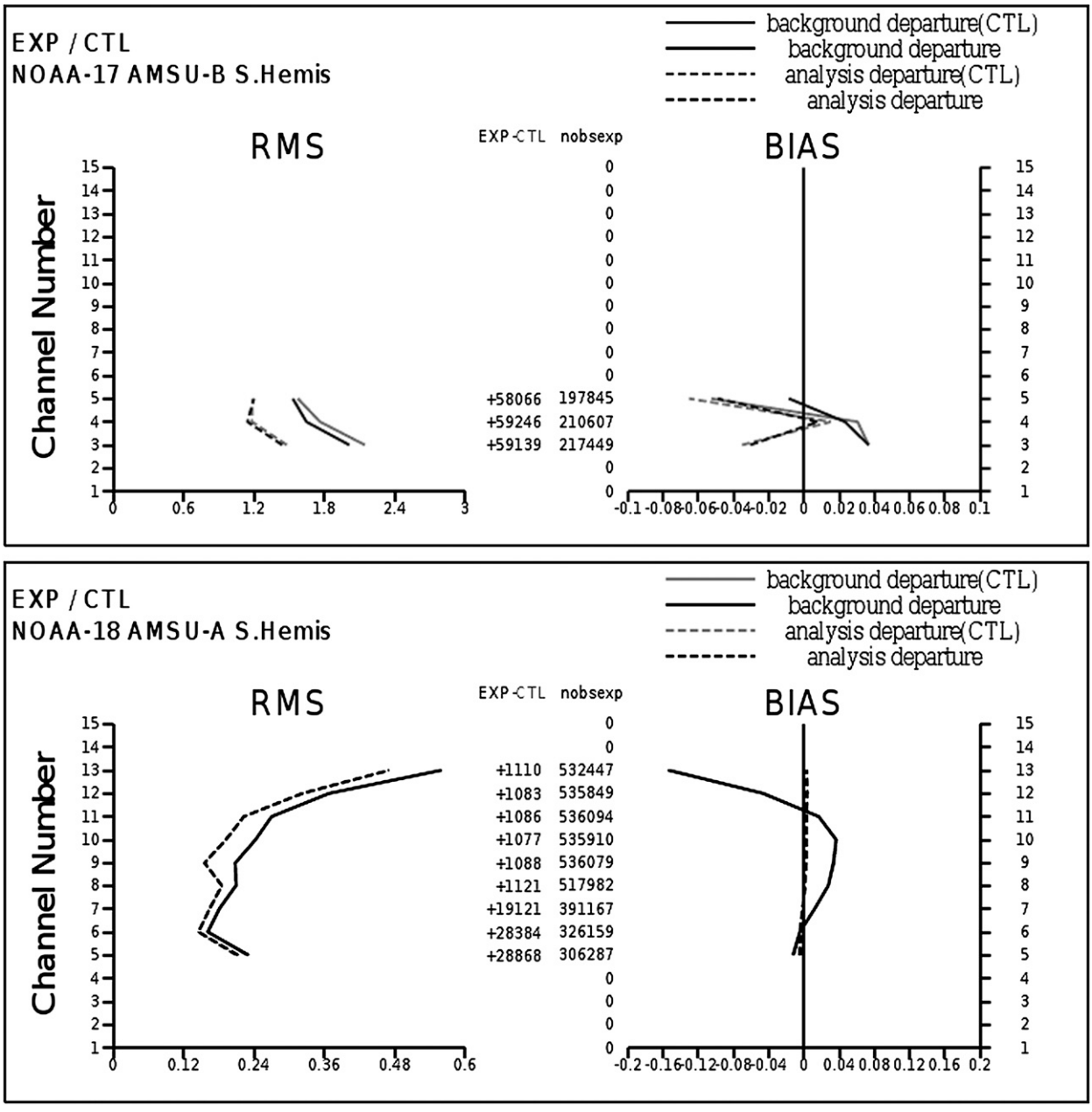

FIG. 7. As in Fig. 6, but for the Southern Hemisphere.

suited for humidity sounding channels than the emissivity at 89 GHz. The impact of this approach in the context of two assimilation experiments within the ARPEGE global model is discussed hereafter.

3. Assimilation experiments

a. Experimental setup

This study relies on the multi-incremental four-dimensional variational data assimilation (4DVAR) scheme of Météo-France's ARPEGE assimilation and forecast system, developed in collaboration with the European Centre for Medium-Range Weather Forecasts (ECMWF) (Courtier et al. 1994; Veersé and Thépaut 1998; Rabier et al. 2000). As in most assimilation systems, ARPEGE seeks a state of the atmosphere that represents the optimal balance between observations and the background information (short-range forecast from a previous analysis). It is based on the 2010 operational cy35t2 cycle version ARPEGE system and consists of a 6-hourly cycle assimilation system, 70 vertical levels (from 17 m to 70 km), and a horizontal resolution that

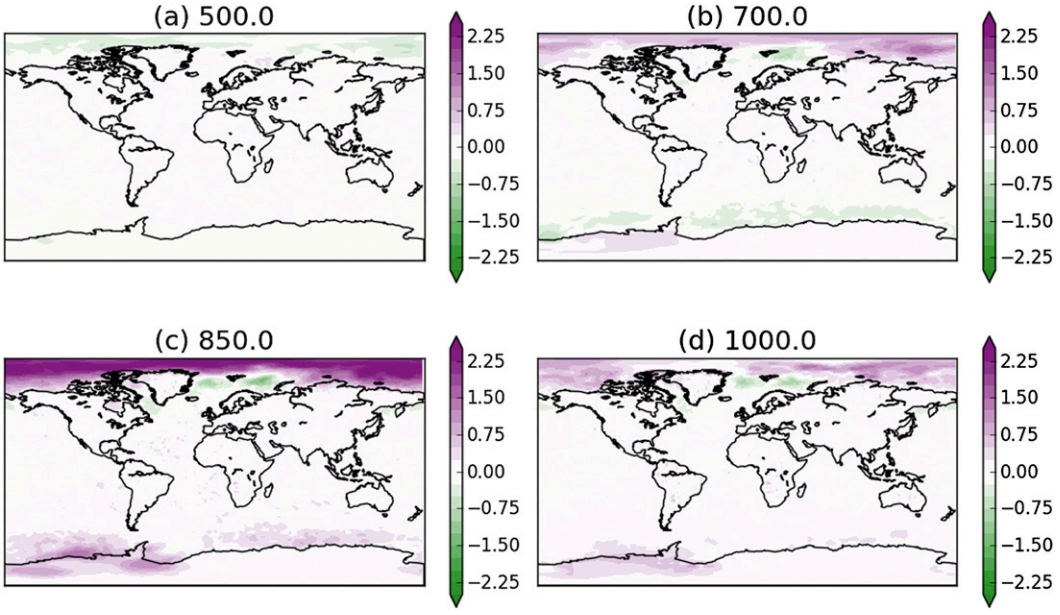

FIG. 8. Mean analysis difference (EXP − CTL) in temperature at (a) 500, (b) 700, (c) 850, and (d) 1000 hPa. Data were averaged over 20 days (from 5 to 25 Jan).

varies from 15 km over Europe to 55 km over the antipodes. The system uses conventional observations (surface stations, buoys, upper-air measurements, radiosondes) and satellite observations (e.g., atmospheric motion vectors from geostationary satellites, radiances from polar-orbiting satellites). For satellite data, ARPEGE uses an adaptive variational bias correction method, which is applied to bias correct satellite observations (Auligné et al. 2007). The analyses–forecasts from both assimilation experiments based on this version of the ARPEGE system are compared. The first experiment (called CTL hereafter) is representative of the operational version of the Météo-France NWP model, whereas the second experiment (called EXP hereafter) uses the sea ice emissivity parameterization and assimilates a selection of AMSU channels above polar regions. Both experiments only differ in their treatment of the sea ice emissivity and their assimilation, or not, of a selection of AMSU channels. In CTL, no AMSU-B/Microwave Humidity Sounder (MHS) observations are assimilated over sea ice, and sea ice emissivity is simply equal to 0.99. For AMSU-A, CTL uses Grody's (1988) algorithm to calculate sea ice emissivity using precalculated emissivities and AMSU-A brightness temperatures (from 23.8 to 89 GHz). Characteristics of the experiments and of the AMSU data used are summarized in Tables 2 and 3, respectively. Note that several conditions must be met before an observation is considered suitable for assimilation, including a quality control test that uses background departures (observations minus simulations using background fields, FGs) from AMSU-A channel 4 and AMSU-B channel 2 to reject data with strong cloud contamination. AMSU-B channel 2 FG departures should be within ±5 K and AMSU-A channel 4 FG departures should be within ±0.7 K. As a consequence, any improvement in FG departures for these two channels (which are sensitive to the surface) would help the assimilation of sounding channels. For instance, if a QC test fails for one of AMSU-B channel 2 pixels, then all AMSU-B pixels for the same location are rejected. Experiments were run over 50 days starting on 15 December 2008 and produced global analyses 4 times per day and 4-day forecasts every day at 0000 UTC. The initial conditions were taken from the operational analysis at 1800 UTC on 14 December 2009.

b. *Impacts on analyses*

For EXP, which benefits from the assimilation of additional data over sea ice, the model fit to assimilated observations is generally improved. Given the rather large increase in the number of AMSU observations that are assimilated over sea ice (about 30% more), the fits of the AMSU observations compared to the FGs or the analysis are also improved. Figure 6 shows biases (left) and RMS errors (right) for the background departures (FGs) (solid) and for the analysis departures (dashed) for assimilated observations from AMSU-B measurements taken aboard the *National Oceanic and Atmospheric Administration-17* (*NOAA-17*) satellite (top)

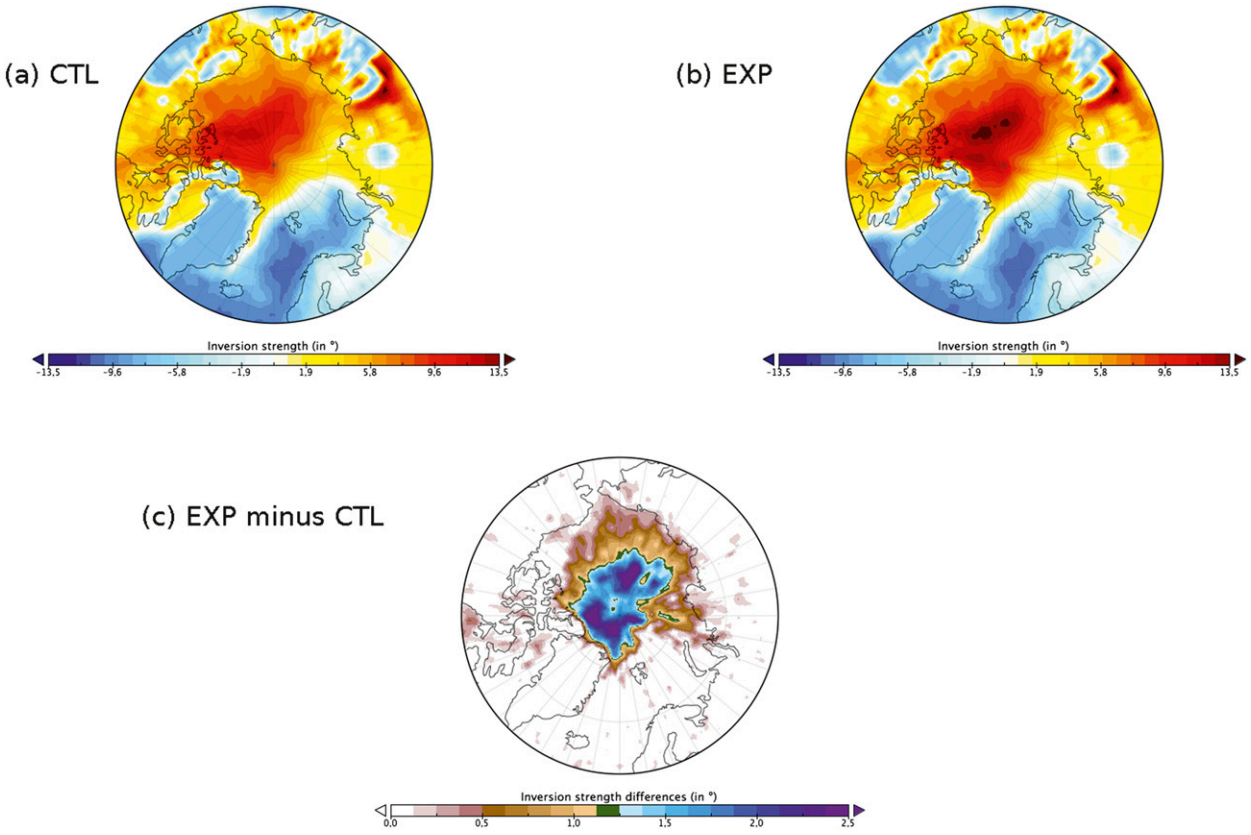

FIG. 9. Average inversion strength for (a) CTL (5–25 Jan 2009), (b) EXP (same period), and (c) mean differences using positive inversion strengths (EXP − CTL).

and from *NOAA-18* AMSU-A results (bottom). In Fig. 6 the results for EXP are plotted in black and for CTL in gray, for January 2009 over the Northern Hemisphere. Figure 7 is similar to Fig. 6 but for the Southern Hemisphere. Both figures clearly show the large increases in the numbers of assimilated observations over polar regions: over 30% for AMSU-B observations and over 10% for AMSU-A. In spite of this significant increase in data, the model fit for the FGs and the analysis to the observations is not degraded; rather, it is even improved, especially for the AMSU-B observations. The assimilation of microwave observations over sea ice markedly modifies atmospheric analyses of these regions at many levels. It leads to an increase in air temperature in the polar regions from the surface to about 500 hPa. This warming is stronger in the Northern Hemisphere and at levels between 800 and 900 hPa with average differences close to 2 K. Close to the surface level, EXP shows a slightly smaller effect on temperature with a mean increase of about 0.5 K with respect to CTL. Figures 8a–d show mean temperature analysis difference maps (EXP minus CTL) at 500, 700, 850, and 1000 hPa. At 500 hPa, EXP brings a slight decrease in temperature (0.5 K) to the Arctic Circle, together with a slight increase in temperature near the Greenland Sea (less than 0.5 K). Above 500 hPa, the EXP effect on temperature becomes negligible. At 700 and 850 hPa, a strong increase in temperature over the Arctic Circle can be observed with a slight decrease in temperature near the Greenland Sea and the Barents Sea. This effect is maximal at 850 hPa with warming average values exceeding 2 K in the Northern Hemisphere and 1 K in the Southern Hemisphere. One can note that this increase is consistent with findings from the Concordiasi results, showing that the ARPEGE model is too cold over sea ice (Cohn et al. 2013). Furthermore, Tjernstrom and Graversen (2009) studied the vertical thermal structure of the lower troposphere using in situ data and 40-yr ECMWF Re-Analysis (ERA-40) data and showed in particular that ERA-40 temperatures are too cold in the upper half of the troposphere. By differentiating the temperature at the 850-hPa level and near the surface (1000 hPa), a proxy for the Arctic inversion strength, which is one the dominant features of the Arctic atmosphere, can be obtained. A working knowledge of the inversion strength, frequency, and depth is of high

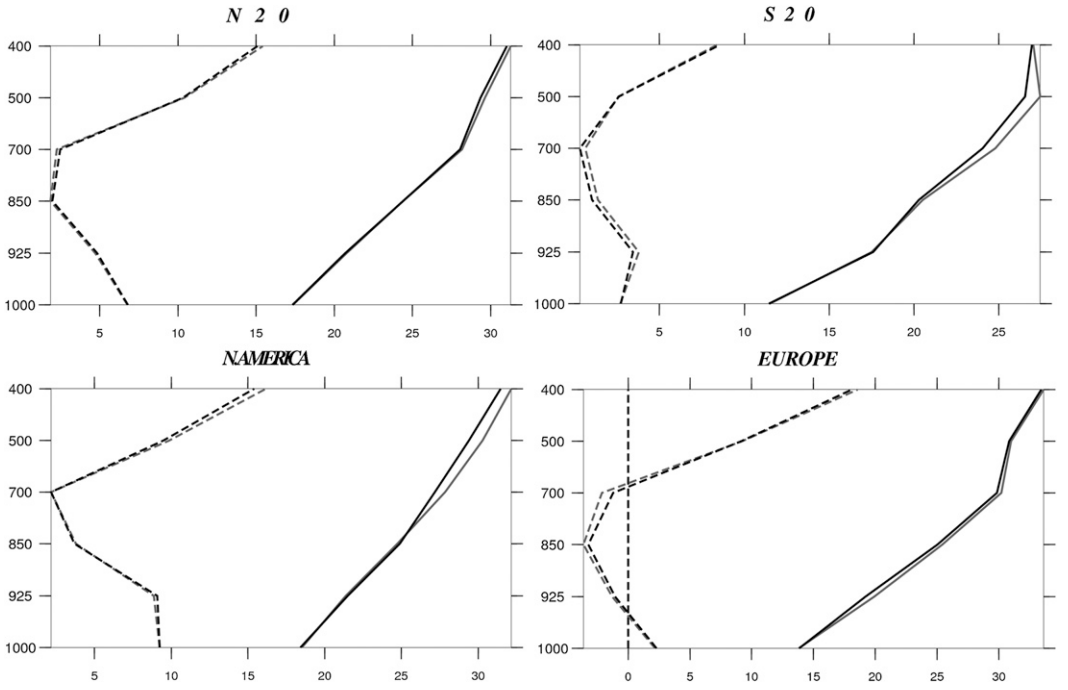

FIG. 10. RMSE (solid lines) and mean bias (dashed lines) for relative humidity differences (%) between the 96-h forecasts of CTL (gray) and EXP (black), with the radiosonde providing the target observations. Results are given for four different domains: the Northern Hemisphere, the Southern Hemisphere, Europe, and North America.

importance for understanding high-latitude climate change. In their study, Tjernstrom and Graversen (2009) showed that the inversion strength in winter in ERA-40 is close to 10 K, but is too weak compared to sounding data. Medeiros et al. (2011) showed that the Arctic inversion representation in climate models is still below climate study requirements: this variable is overestimated in some climate models and is spatially biased in some others. Figures 9a and 9b show average inversion strengths using 20 days (5–25 January) of CTL and EXP data, respectively. On average, the strength of the inversion is around 10 K with some spatial variations. The assimilation of AMSU data over sea ice enhances the inversion strength throughout the region of the Arctic ice cap by about 1–2.5 K (see Fig. 9c) and the RMSs of the inversion strength differences (EXP-CTL) vary from 0.5 to 1.5 K (not shown). We do not have independent data to verify this change. Only changes in temperature, as noted earlier, seem to go in the right direction with respect to various studies reporting some cold bias patterns in NWP models in the regions of sea ice. The change in inversion strength is an important issue that deserves special consideration over a longer period of assimilation to better understand the impacts of the observations. Modifications with regard to moisture seem to be of a less quantitative nature for the Northern Hemisphere. However, there is a tendency to moisten the air above the Antarctic ice below 700 hPa. As for wind, the analysis change appears to vary with the pressure levels and the location (not shown). Overall, the impact on the analysis seems to affect the Northern Hemisphere more as the preponderance of the sea ice is to be found in this hemisphere during the period of study. The analysis change is associated with high values of standard deviations, especially in the Northern Hemisphere. It is difficult to say at this stage which one of the two experiments provides the best atmospheric analyses in the absence of independent measurements over sea ice. A possible answer is to examine the model fit to observations (for FGs and analyses). These diagnostics favor EXP (as shown in the beginning of this section). Another way of evaluating the analyses is to examine forecasts made by models that use atmospheric analyses as initial conditions based on the assumption that forecasts are best when based on improved initial conditions. An evaluation of EXP forecasts versus CTL is presented in the next section.

c. *Impact on forecasts*

An evaluation of the forecast performances of CTL and EXP was made by means of verification scores (up to 4 days) for mass, wind, relative humidity, and temperature fields. The forecast root-mean-square errors (RMSEs) for each field were calculated using

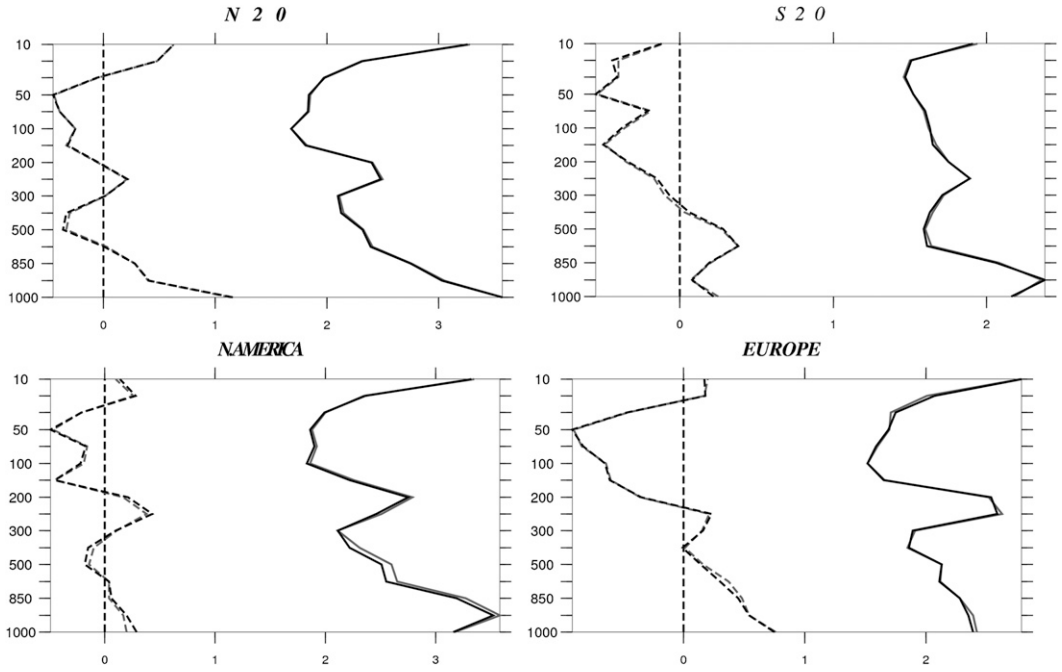

FIG. 11. As in Fig. 10, but for temperature (K).

simulations from 26 December 2008 to 3 February 2009, with radiosonde observations as target estimations. It was found that medium-range forecasts of EXP are better than those of CTL with better biases and RMSEs, especially for Europe and North America. Figure 10 shows RMSEs (solid lines) and mean biases (dashed lines) for relative humidity between the 96-h forecasts of CTL (red) and EXP (black). Results are given for four

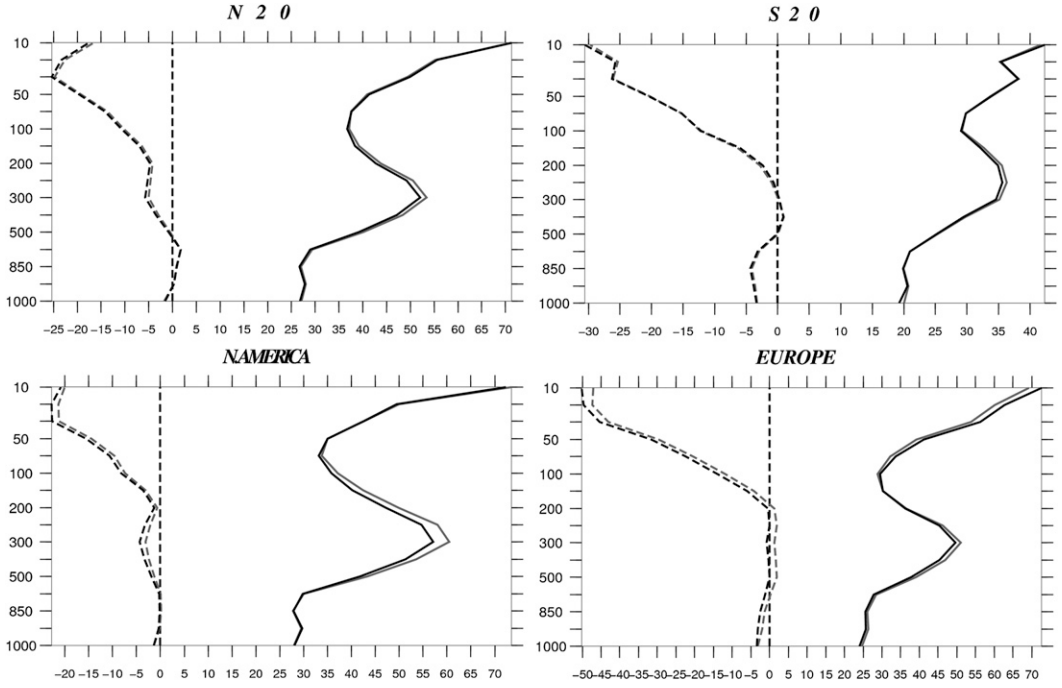

FIG. 12. As in Fig. 10, but for geopotential height (m).

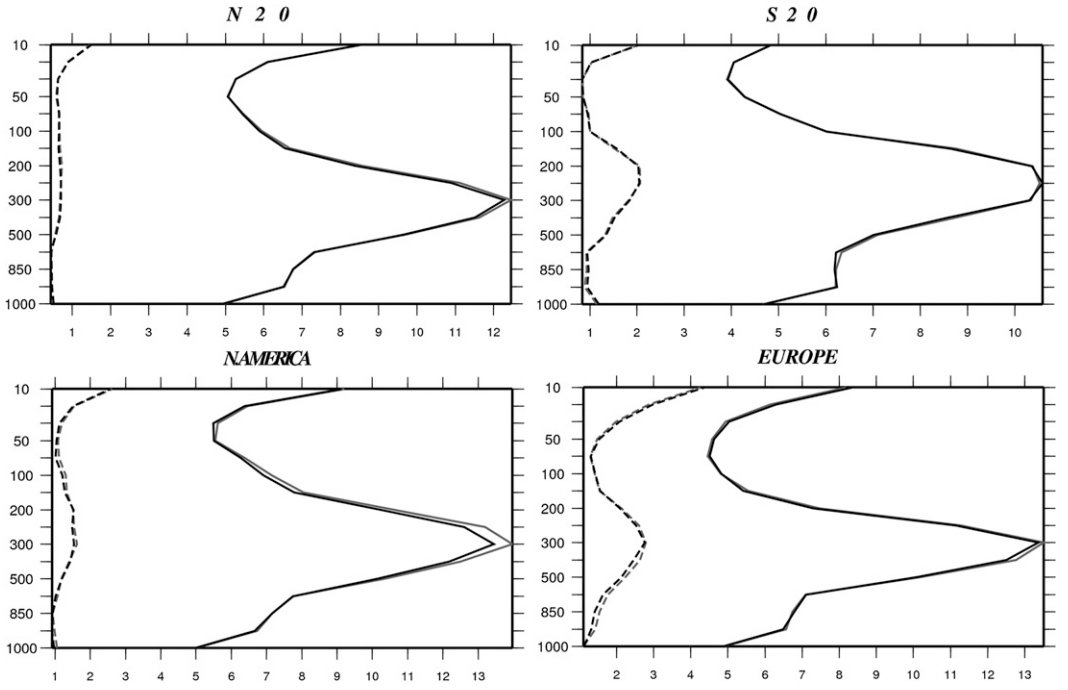

FIG. 13. As in Fig. 10, but for wind ($m\,s^{-1}$).

different domains where the scores were statistically significant (at the 90% confidence level or better): Europe, North America, the Northern Hemisphere (north of 20°N), and the Southern Hemisphere (south of 20°S). Figures 11, 12, and 13 are similar to Fig. 10 but for temperature, geopotential height, and wind speed, respectively. From these figures, it can be seen that, in EXP, the 96-h forecasts for temperature, humidity, and wind are improved when compared to CTL. Additional verification scores were calculated using as a target the analysis of the experiment assimilating the highest number of observations (EXP). The forecast scores presented next are obtained by computing the difference between the RMS forecast errors between EXP and CTL. For each experiment, forecasts were verified against a target analysis. Positive (negative) impacts of EXP are associated with negative (positive) RMS differences. Results show that 24-h forecast improvements are concentrated near the poles and relate to several levels of the atmosphere. Figures 14a–d shows RMS forecast error difference in geopotential height at 500 hPa for 24, 48, 72, and 96 h. The forecasts are verified against the analysis of EXP (which assimilates the largest number of observations) and are for the period 5–25 January 2009. The general improvement of the forecast can be observed at all forecast ranges but with some limited regions where the impact is negative. At 96 h, polar regions still benefit from the assimilation of microwave data, with the effect propagating toward the midlatitudes.

4. Conclusions

Limited observations are assimilated over sea ice surfaces. The imperfect representation of the surface emissivity and temperature of sea ice makes it difficult to carry out assimilation trials. Within the framework of the Concordiasi project, modeling studies have been conducted to improve the sea ice emissivity at microwave frequencies for the assimilation of observations from AMSU-A and AMSU-B/MHS over polar regions. The emissivity of sea ice was calculated directly from microwave observations by removing the atmospheric contribution to the measured radiometric signal. The emissivity was derived at 23, 31, 50, 89, and 150 GHz and its temporal and spatial variabilities were analyzed. Complementary sea ice products were used to better understand the variability of the emissivity including its variability with frequency. The analysis of the emissivity enabled a parameterization of surface emissivity with a correction made to the 89-GHz frequency to be more consistent with the AMSU-B humidity channels. For AMSU-A channels, the 50-GHz emissivity of ice was found to be suitable for temperature sounding channels. To evaluate the impact of the sea ice emissivity parameterization, two global assimilation and forecast experiments were run. It has been shown that the assimilation of AMSU measurements was possible over sea ice areas, with very good simulations of the radiative transfer model RTTOV. The assimilation of these data improves

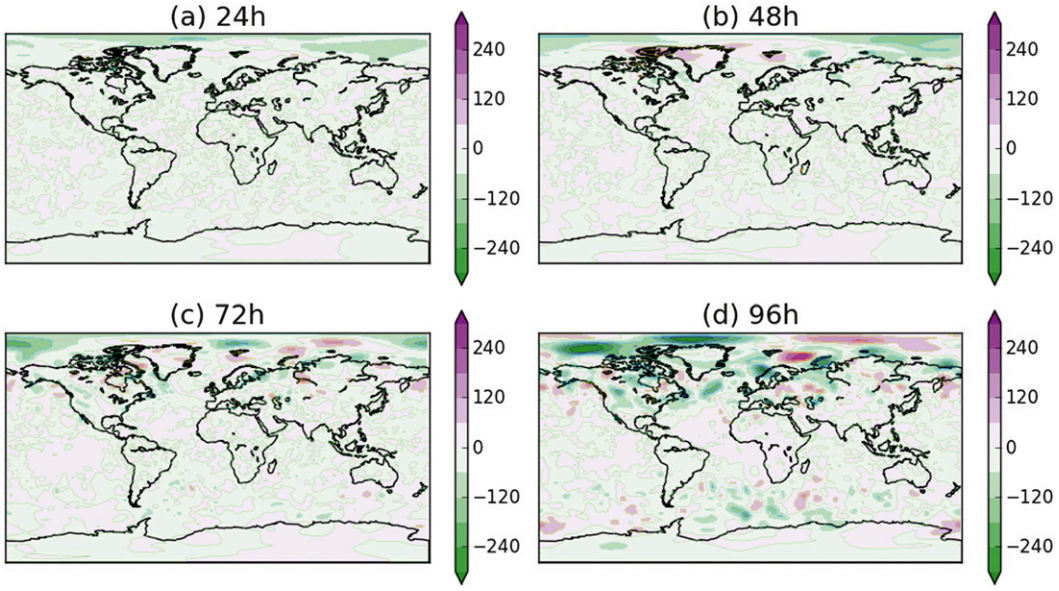

FIG. 14. Forecast scores at 500 hPa for geopotential height presented for four forecast ranges. Each panel shows the difference in RMS (EXP − CTL), with RMS errors being computed between forecasts at (a) 24, (b) 48, (c) 72, and (d) 96 h and the verifying analysis. The impact of AMSU assimilation is positive (negative) for negative (positive) RMS differences. The period is 5–25 Jan 2009 (m ×100).

the fit to the assimilated data as compared to background or analysis. The fit to the AMSU observations was improved with nearly 30% more assimilated AMSU-B data (more than 10% for AMSU-A). The assimilation of these data produces a significant change in the atmospheric analyses over polar areas (in particular those of temperature and humidity). The effect on temperature results in a warming of the lower troposphere, which is more pronounced around 850 hPa and weaker close to the surface. This leads to an increase in the Arctic inversion strength over the Arctic ice cap of almost 2 K. Forecasts were generally improved especially over Europe and North America for forecast ranges greater than 48 h. Finally, it must be stressed that the Météo-France assimilation system has been using the sea ice emissivity parameterization operationally for AMSU-A and AMSU-B since November 2010 and during the Concordiasi experiment at the end of 2010. A very positive forecast impact from AMSU-B data over sea ice was found in the southern polar area (N. Saint-Ramond, personal communication). contrary to other NWP centers, which do not use these data optimally.

Acknowledgments. The authors would like to deeply thank three anonymous reviewers for their numerous constructive insights and especially one anonymous referee for pointing out the potential importance of the assimilation of microwave data for the Arctic inversion. The authors wish to thank Jean Maziejewski for his help in revising the manuscript.

REFERENCES

Andersen, S., and Coauthors, 2012: Sea ice product manual. EUMETSAT/OSI SAF, 38 pp. [Available online at http://osisaf.met.no/docs/osisaf_ss2_pum_ice-conc-edge-type_v3p8.pdf.]

Auligné, T., A. P. McNally, and D. P. Dee, 2007: Adaptive bias correction for satellite data in a numerical weather prediction system. *Quart. J. Roy. Meteor. Soc.,* **133,** 631–642.

Bouchard, A., F. Rabier, V. Guidard, and F. Karbou, 2010: Enhancement of satellite data assimilation over Antarctica. *Mon. Wea. Rev.,* **138,** 2149–2173.

Choudhury, B. J., 1993: Reflectivities of selected land surface types at 19 and 37 GHz from SSM/I observations. *Remote Sens. Environ.,* **46,** 1–17.

Cohn, S. A., and Coauthors, 2013: Driftsondes: Providing in situ, long-duration, dropsonde observations over remote regions. *Bull. Amer. Meteor. Soc.,* **94,** 1661–1674.

Courtier, P., J. N. Thépaut, and A. Hollingsworth, 1994: A strategy for operational implementation of 4D-Var using an incremental approach. *Quart. J. Roy. Meteor. Soc.,* **120,** 1367–1387.

English, S., 2008: The importance of accurate skin temperature in assimilating radiances from satellite sounding instruments. *IEEE Trans. Geosci. Remote Sens.,* **46,** 403–408.

Eyre, J., 1991: A fast radiative transfer model for satellite sounding systems. ECMWF Tech. Memo. 176, 28 pp. [Available from ECMWF, Shinfield Park, Reading RG2 9AX, United Kingdom.]

Felde, G. W., and J. D. Pickle, 1995: Retrieval of 91 and 150 GHz earth surface emissivities. *J. Geophys. Res.,* **100,** 20 855–20 866.

Goodrum, G., K. B. Kidwell, and W. Winston, cited 2012: The NOAA KLM users guide. NOAA/NESDIS/NCDC. [Available online at http://www2.ncdc.noaa.gov/docs/klm/index.htm.]

Grody, N. C., 1988: Surface identification using satellite microwave radiometers. *IEEE Trans. Geosci. Remote Sens.,* **26,** 850–859.

Guedj, S., F. Karbou, F. Rabier, and A. Bouchard, 2010: Microwave land emissivity over Antarctica: Impact of the surface approximation. *IEEE Trans. Geosci. Remote Sens.,* **48,** 1976–1985, doi:10.1109/TGRS.2009.2036254.

Jones, A. S., and T. H. Vonder Haar, 1997: Retrieval of microwave surface emittance over land using coincident microwave and infrared satellite measurements. *J. Geophys. Res.,* **102** (D12), 13 609–13 626.

Karbou, F., and C. Prigent, 2005: Calculation of microwave land surface emissivities from satellite observations: Validity of the specular approximation over snow-free surfaces? *IEEE Trans. Geosci. Remote Sens. Lett.,* **2,** 311–314, doi:10.1109/LGRS.2005.847932.

——, ——, L. Eymard, and J. Pardo, 2005: Microwave land emissivity calculations using AMSU-A and AMSU-B measurements. *IEEE Trans. Geosci. Remote Sens.,* **43,** 948–959.

——, E. Gérard, and F. Rabier, 2006: Microwave land emissivity and skin temperature for AMSU-A and -B assimilation over land. *Quart. J. Roy. Meteor. Soc.,* **132,** 2333–2355, doi:10.1256/qj.05.216.

Kongoli, C., S. Boukabara, B. Yan, F. Weng, and R. Ferraro, 2010: A new sea-ice concentration algorithm based on microwave surface emissivities application to AMSU measurements. *IEEE Trans. Geosci. Remote Sens.,* **49,** 175–189, doi:10.1109/TGRS.2010.2052812.

Mathew, N., G. Heygster, C. Melsheimer, and L. Kaleschke, 2008: Surface emissivity of polar regions at AMSU window frequencies. *IEEE Trans. Geosci. Remote Sens.,* **46,** 2298–2306, doi:10.1109/TGRS.2008.916630.

——, ——, and ——, 2009: Surface emissivity of the Arctic sea ice at AMSR-E frequencies. *IEEE Trans. Geosci. Remote Sens.,* **47,** 4115–4124, doi:10.1109/TGRS.2009.2023667.

Matricardi, M., F. Chevallier, G. Kelly, and J. Thépaut, 2004: Channel selection method for IASI radiances. *Quart. J. Roy. Meteor. Soc.,* **130,** 153–173.

Matzler, C., 2005: On the determination of surface emissivity from satellite observations. *IEEE Geosci. Remote Sens. Lett.,* **2,** 160–163, doi:10.1109/LGRS.2004.842448.

——, and P. W. Rosenkranz, 2007: Dependence of microwave brightness temperature on bistatic surface scattering: Model functions and application to AMSU-A. *IEEE Geosci. Remote Sens.,* **45,** 2130–2138, doi:10.1109/TGRS.2007.898089 7.

Medeiros, B., C. Deser, R. Tomas, and J. Kay, 2011: Arctic inversion strength in climate models. *J. Climate,* **24,** 4733–4740.

Prigent, C., W. B. Rossow, and E. Matthews, 1997: Microwave land surface emissivities estimated from SSM/I observations. *J. Geophys. Res.,* **102,** 21 867–21 890.

——, J. Wigneron, B. Rossow, and J. R. Pardo, 2000: Frequency and angular variations of land surface microwave emissivities: Can we estimate SSM/T and AMSU emissivities from SSM/I emissivities? *IEEE Trans. Geosci. Remote Sens.,* **38,** 2373–2386.

——, F. Chevallier, F. Karbou, P. Bauer, and G. Kelly, 2005: AMSU-A surface emissivities for numerical weather prediction assimilation schemes. *J. Appl. Meteor.,* **44,** 416–426.

Rabier, F., H. Jarvinen, E. Klinker, J. F. Mahfouf, and A. Simmons, 2000: The ECMWF operational implementation of four-dimensional variational assimilation. I: Experimental results with simplified physics. *Quart. J. Roy. Meteor. Soc.,* **126,** 1143–1170.

——, and Coauthors, 2010: The Concordiasi project in Antarctica. *Bull. Amer. Meteor. Soc.,* **91,** 69–86.

——, and Coauthors, 2013: The Concordiasi field experiment over Antarctica: First results from innovative atmospheric measurements. *Bull. Amer. Meteor. Soc.,* **94,** ES17–ES20.

Saunders, R. W., M. Matricardi, and P. Brunel, 1999: An improved fast radiative transfer model for assimilation of satellite radiance observations. *Quart. J. Roy. Meteor. Soc.,* **125,** 1407–1425.

Tjernstrom, M., and R. Graversen, 2009: The vertical structure of the lower Arctic troposphere analyzed from observations and the ERA-40 reanalysis. *Quart. J. Roy. Meteor. Soc.,* **135,** 431–443.

Veersé, F., and J. N. Thépaut, 1998: Multiple truncation incremental approach for four-dimensional variational data assimilation. *Quart. J. Roy. Meteor. Soc.,* **124,** 1889–1908.